



**Photoluminescence studies of bandedge transitions in GaN epitaxial layers grown by plasmaassisted molecular beam epitaxy**

G. D. Chen, M. Smith, J. Y. Lin, H. X. Jiang, A. Salvador, B. N. Sverdlov, A. Botchkarov, and H. Morkoc

Citation: [Journal of Applied Physics](#) **79**, 2675 (1996); doi: 10.1063/1.361138

View online: <http://dx.doi.org/10.1063/1.361138>

View Table of Contents: <http://scitation.aip.org/content/aip/journal/jap/79/5?ver=pdfcov>

Published by the [AIP Publishing](#)

---



## Re-register for Table of Content Alerts

Create a profile.



Sign up today!



# Photoluminescence studies of band-edge transitions in GaN epitaxial layers grown by plasma-assisted molecular beam epitaxy

G. D. Chen,<sup>a)</sup> M. Smith, J. Y. Lin, and H. X. Jiang  
*Department of Physics, Kansas State University, Manhattan, Kansas 66502-2601*

A. Salvador, B. N. Sverdlov, A. Botchkarov, and H. Morkoc  
*Materials Research Laboratory and Coordinated Science Laboratory,  
University of Illinois at Urbana-Champaign, Urbana, Illinois 61801*

(Received 15 September 1995; accepted for publication 16 November 1995)

Continuous-wave and time-resolved photoluminescence spectroscopies have been employed to study the band-edge transitions in GaN epitaxial layers grown by plasma assisted molecular beam epitaxy. In addition to the neutral-donor-bound exciton transition (the  $I_2$  line), a transition line at about 83 meV below the band gap has been observed in an epitaxial layer grown under a lower plasma power or growth rate. This emission line has been assigned to the band-to-impurity transition resulting from the recombination between electrons bound to shallow donors and free holes ( $D^0, h^+$ ). Systematic studies of these optical transitions have been carried out under different temperatures and excitation intensities. The temperature variation of the spectral peak position of the ( $D^0, h^+$ ) emission line differs from the band gap variation with temperature, but is consistent with an existing theory for ( $D^0, h^+$ ) transitions. The dynamic processes of the ( $D^0, h^+$ ) transition have also been investigated and subnanosecond recombination lifetimes have been observed. The emission energy and the temperature dependencies of the recombination lifetime have been measured. These results have provided solid evidence for the assignment of the ( $D^0, h^+$ ) transition and show that the motions of the free holes which participated in this transition are more or less restricted in the plane of the epitaxial layer at temperatures below 140 K and that the thermal quenching of the emission intensity of this transition is due to the dissociation of neutral donors. Our results show that time-resolved photoluminescence spectroscopy can be of immense value in understanding the optical recombination dynamics in GaN. © 1996 American Institute of Physics. [S0021-8979(96)07804-6]

## I. INTRODUCTION

GaN and  $\text{Al}_x\text{Ga}_{1-x}\text{N}$  wide band gap semiconductors have been intensively studied<sup>1-6</sup> recently for applications in two areas: (1) optical devices, including blue-UV light-emitting diodes (LED) and laser diodes. The fabrication of a GaN commercial blue LED with the highest luminosity reported to date is just one example;<sup>7</sup> (2) electronic devices, including devices which can operate in hostile environments such as high temperature and under high radiation doses and under extreme conditions such as high frequency and high power. One such example is the fabrication of  $\text{Al}_x\text{Ga}_{1-x}\text{N}/\text{GaN}$  metal-semiconductor field-effect transistors (MESFETs) with high cutoff frequencies for microwave and millimeter wave applications.<sup>8,9</sup> In particular, because GaN and AlN form a continuous alloy system whose direct band gap at room temperature ranges from 3.4 to 6.2 eV, their applications for many novel optical devices are very promising.

There has been a considerable amount of research effort directed toward the understanding of the optical properties of GaN and  $\text{Al}_x\text{Ga}_{1-x}\text{N}$ . The band-edge luminescence from GaN crystals at low temperatures is known to consist of lines resulting from excitons (either free or bound excitons) and donor-to-acceptor (DAP) transitions. The identification of

free and bound exciton and impurity transitions was made by Pankove *et al.*<sup>10</sup> Dingle *et al.*,<sup>11-13</sup> and subsequently by many other researchers.<sup>14-20</sup> Their work has provided a reasonable account of the optical properties of wurtzite GaN. However, many basic physical parameters, which are important in fundamental physics as well as in practical applications, are still unknown. In particular, the study of optical recombination dynamics in these materials are scarce. There is no doubt that the understanding of the carrier dynamics in GaN and  $\text{Al}_x\text{Ga}_{1-x}\text{N}$  can provide immense value in designing and optimizing optoelectronic devices based on the GaN system as well as in optimizing material growth conditions. This has been proven previously for materials such as GaAs and ZnSe.

Most recently, we have performed a series of studies on the dynamic processes of optical transitions in GaN epitaxial layers deposited by different techniques under different conditions. These include intrinsic exciton recombination in superior quality as well as high-purity epitaxial GaN layers deposited by the new molecular beam epitaxy (MBE) and metalorganic chemical vapor deposition (MOCVD) techniques,<sup>21,22</sup> impurity-bound exciton recombination in  $n$  and  $p$  type layers deposited by MOCVD,<sup>23</sup> and a band-to-impurity recombination in  $n$ -type layers deposited earlier by plasma-assisted MBE.<sup>24</sup> In this work, the photoluminescence properties of the neutral-donor-bound exciton transition ( $I_2$ ) and the band-to-impurity transition ( $D^0, h^+$ ) in  $n$ -type

<sup>a)</sup>Permanent address: Department of Applied Physics, Xi'an Jiaotong University, People's Republic of China.

TABLE I. Summary data of two GaN samples under investigation.

	Thickness ( $\mu\text{m}$ )	ECR power (W)	Growth rate ( $\mu\text{m}/\text{h}$ )	Mobility ( $\text{cm}^2/\text{V s}$ ) (300 K)	Free electron concentration (300 K)	Dominant emission lines (10 K) (eV)
Sample A (A1180)	3	120	0.135	150	$10^{18} \text{ cm}^{-3}$	3.474
Sample B (A1187)	3	70	0.11	10	$2.6 \times 10^{17} \text{ cm}^{-3}$	3.474, 3.422–3.415, 3.338

GaN layers deposited by plasma-assisted MBE have been studied in detail by extending the measurement temperature range from 10 to 300 K and the excitation intensity variation by 3 orders of magnitude. The temperature dependence of the ( $D^0$ ,  $h^+$ ) emission intensity reveals the thermal quenching process of this transition line, which is related to ionization of neutral donors. The dynamics of this emission line have been investigated by time-resolved spectroscopy. The emission energy and temperature dependencies of the recombination lifetime have been measured. These results have provided solid evidence for the assignment of the ( $D^0$ ,  $h^+$ ) transition and show that the motions of the free holes which participated in this transition are more or less restricted in the plane of the epitaxial layer at temperatures below 140 K. Our results indicate that the shallow donor impurities involved in the ( $D^0$ ,  $h^+$ ) transition are different from the native donors of nitrogen vacancies and are not responsible for the high free electron concentrations in GaN.

## II. EXPERIMENT

The wurtzite GaN samples used in the present work were grown by the plasma-assisted MBE described earlier on a sapphire ( $\text{Al}_2\text{O}_3$ ) substrate with a 50 nm AlN buffer layer.<sup>24</sup> The substrate temperature during the growth was 750 °C. An electron cyclotron resonance (ECR) source provided the reactive nitrogen while Ga and Al were evaporated using conventional effusion cells. Sample A was grown under a microwave plasma power of 120 W and has a room temperature electron concentration ( $n$ ) of about  $10^{18} \text{ cm}^{-3}$  and mobility of about  $150 \text{ cm}^2/\text{V s}$  as determined by Hall measurement. Sample B was grown under a lower microwave plasma power of 70 W at a lower growth rate than sample A and has a room temperature electron concentration of about  $2.6 \times 10^{17} \text{ cm}^{-3}$  and mobility of about  $10 \text{ cm}^2/\text{V s}$ . In sample A, the dominant emission line was associated with the recombination of the neutral-donor-bound exciton (the  $I_2$  line). In sample B, in addition to the  $I_2$  line, there were two other emission lines near 3.420 and 3.338 eV. The growth conditions, sample parameters obtained at room temperature, and the dominant low temperature emission lines of these two samples have been summarized in Table I.

For photoluminescence measurements, samples were attached to copper sample holders and placed inside a closed-cycle He refrigerator with a temperature variation from 10 to 320 K. A temperature controller enabled us to stabilize the temperature to within 0.1 K. Photoluminescence spectra were collected in a reflecting mode. Excitation pulses of

about 7 ps at a repetition rate of 9.5 MHz were provided by a cavity-dumped dye laser (Coherent 702-2CD) with Rhodamine 6G dye solution, which was pumped by a yttrium–aluminum–garnet (YAG) laser (Coherent Antares 76) with a frequency doubler. The output from the dye laser was frequency doubled again by a second frequency doubler to provide tunability in the UV region. The laser output after the second doubler has an average power of about 20 mW, a tunable photon energy up to 4.5 eV, and a spectral width of about 0.2 meV. The laser beam size on the sample was about 0.5 mm in diameter. A single-photon counting detection system was used to record the time-resolved photoluminescence spectra. With the use of a deconvolution technique developed by Photon Technology International Inc. (PTI), the overall time resolution of the detection system was about 50 ps. The excitation intensity was controlled by a set of UV neutral density filters with different attenuation parameters  $D$ , and was thus proportional to  $10^{-D}$ .

## III. RESULTS AND DISCUSSION

### A. cw spectra

#### 1. The $I_2$ transition

Figure 1 shows cw emission spectra of sample A ( $n=10^{18} \text{ cm}^{-3}$ ) measured at three representative temperatures, showing one dominant emission line at 3.474 eV at 10 K. The energy position of this emission line is consistent with the transition of excitons bound to neutral donors associated with nitrogen vacancies ( $D^0$ ,  $X$ ) or the  $I_2$  transition line.<sup>2,3</sup> The energy position of the  $I_2$  transition depends slightly on the sample. Different values from 3.470 to 3.476 eV have been reported, which may be related to sample quality, such as impurity concentration and interface morphology. The full width at half-maximum (FWHM) of the  $I_2$  emission line at  $T=10$  K is about 7 meV which indicates that the sample under investigation is of relatively high crystalline quality. For the luminescence spectrum measured at  $T=10$  K, there is a weak peak at about 3.42 eV. The origin of this transition peak will be discussed together with the results obtained from sample B, in which the emission intensity of this transition line is much enhanced. The inset of Fig. 1 shows the excitation intensity dependence of the integrated intensity of the  $I_2$  transition.

The observed  $I_2$  spectral peak position shift with temperature is due to the energy gap variation with temperature. We have plotted the temperature dependence of the  $I_2$  peak position as shown in Fig. 2. The overall feature obtained here

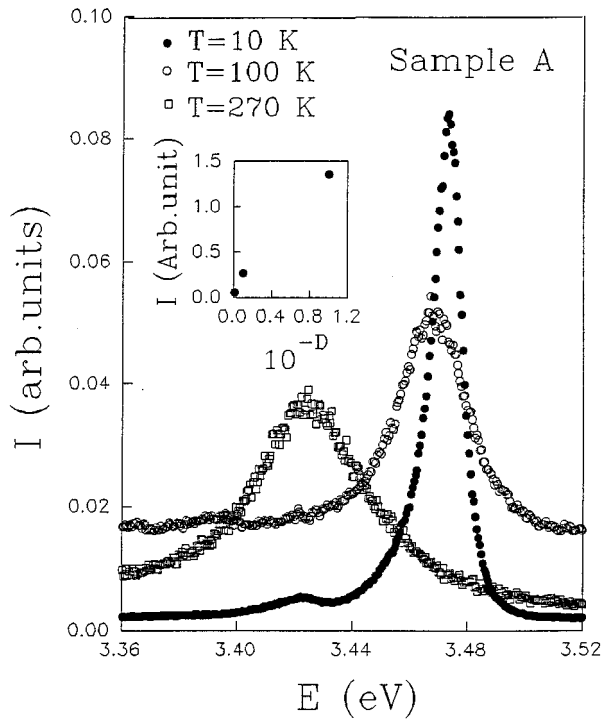


FIG. 1. cw photoluminescence spectra of sample A ( $n=10^{18} \text{ cm}^{-3}$ ) measured at three representative temperatures, which shows that the dominant emission is the  $I_2$  line due to the recombination of excitons bound to neutral donors with the peak position at 3.475 eV at  $T=10 \text{ K}$ . A weak peak at about 3.42 eV at  $T=10 \text{ K}$  is due to band-to-impurity transition ( $D^0, h^+$ ). The inset shows the excitation light intensity ( $I_{\text{exc}}$ ) dependence of the  $I_2$  intensity measured at 10 K.  $I_{\text{exc}}$  is proportional to  $10^{-D}$  with  $D$  being the neutral density filter attenuated parameter. Excitation photon energy was 4.26 eV.

is consistent with previous results.<sup>10,20</sup> Since the energy difference between the  $I_2$  and the energy gap should be independent of temperature, the temperature dependence of the  $I_2$  peak position can be fitted by the temperature dependence of the energy gap by using the empirical equation,

$$E_0(T) = E_0(0) - \alpha T^2 / (\beta + T), \quad (1)$$

where  $E_0(0)$  is the  $I_2$  transition energy at  $T=0 \text{ K}$  and  $\alpha$  and  $\beta$  are constants referred to as Varshni thermal coefficients. The solid curve in Fig. 2 is the least-squares fit of data by using Eq. (1). The fitted values are  $E_0(0) = 3.475 \text{ eV}$ ,  $\alpha = 7.06 \times 10^{-4} \text{ eV/K}$ , and  $\beta = 1.06 \times 10^3 \text{ K}$ .

The FWHM of the  $I_2$  emission line also increases with an increase of temperature, which is due to increased exciton-phonon interactions at higher temperatures. In the inset of Fig. 2, we have plotted the FWHM of the  $I_2$  emission line,  $\Gamma$ , as a function of temperature, which shows that  $\Gamma$  increases linearly with temperature. The temperature dependence of the emission linewidth caused by exciton-phonon interactions has the form<sup>25,26</sup>

$$\Gamma(T) = \Gamma_0 + \gamma_{\text{LA}} T + \gamma_{\text{LO}} / [\exp(E_{\text{LO}}/kT) - 1]. \quad (2)$$

The second and third terms in Eq. (2) are due to the interaction of excitons with the longitudinal acoustic (LA) and longitudinal optical (LO) phonon modes of the lattice.  $\gamma_{\text{LA}}$  and  $\gamma_{\text{LO}}$  are, respectively, the LA coefficient and the LO line-

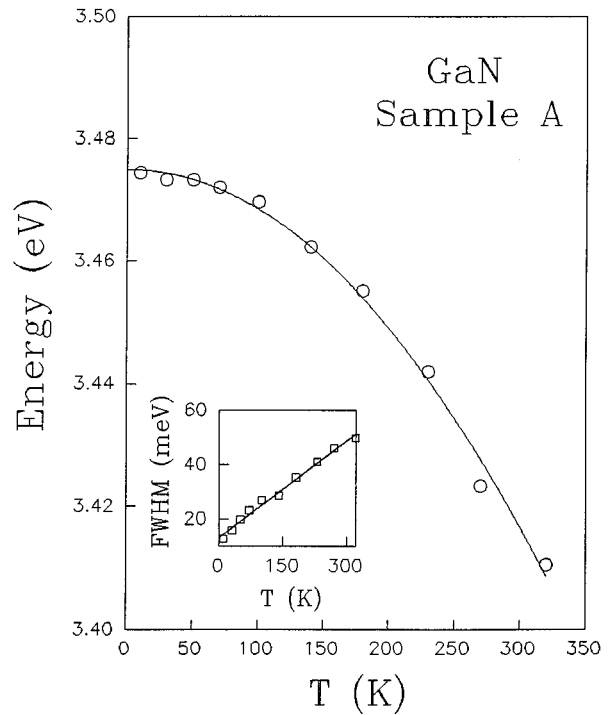


FIG. 2. The temperature dependence of the  $I_2$  emission peak position of sample A as obtained from Fig. 1. The solid line is the least-squares fit of data with Eq. (1). The inset shows the full width at half-maximum (FWHM) of the  $I_2$  transition as a function of temperature, where the solid line is the least-squares fit by a linear relation with temperature of Eq. (3).

width parameters,  $E_{\text{LO}}$  is the LO phonon energy of GaN, and  $\Gamma_0$  is the linewidth at  $T=0 \text{ K}$ , which correlates with the concentration of inhomogeneities or impurities in the sample.

The linear behavior shown in the inset of Fig. 2 implies that the exciton-LA phonon interaction dominates in GaN at temperatures above 40 K, due to the large value of LO phonon energy,  $E_{\text{LO}}$ , in GaN (about 92 meV). By neglecting exciton-LO phonon interactions, Eq. (2) can be reduced to,

$$\Gamma = \Gamma_0 + \gamma_{\text{LA}} T. \quad (3)$$

The solid line in the inset is the least-squares fit of data using Eq. (3) and the fitted values are  $\Gamma_0 = 5 \text{ meV}$  and  $\gamma_{\text{LA}} = 0.16 \text{ meV/K}$ . Thus the results show clearly that the  $I_2$  emission linewidth broadening in MBE grown samples is predominantly determined by acoustic phonon scattering at temperatures above 40 K.

## 2. Band-to-impurity ( $D^0, h^+$ ) transitions

We have also studied the photoluminescence properties of a second sample (B), which was grown at a lower growth rate and has a lower electron mobility than sample A. In Fig. 3, we have plotted the cw luminescence spectra of sample B obtained at 10 K for four different excitation intensities, which shows the  $I_2$  along with two additional emission lines at about 3.42 and 3.34 eV. Each spectrum in Fig. 3 has been normalized to its maximum emission intensity either near 3.42 eV or at the  $I_2$  emission peak position. The spectral peak position of the emission line at around 3.42 eV varies from 3.414 to 3.422 eV depending on excitation intensity

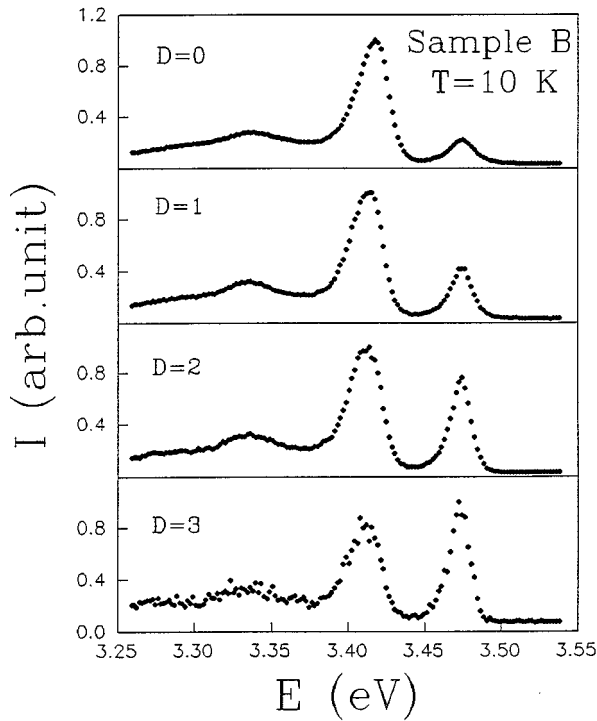


FIG. 3. cw photoluminescence spectra of sample B ( $n=2.6 \times 10^{17} \text{ cm}^{-3}$ ) measured at  $T=10 \text{ K}$  and under different excitation light intensities,  $I_{\text{exc}}$ , with  $I_{\text{exc}}$  being proportional to  $10^{-D}$ . Each spectrum has been normalized to its maximum emission intensity.

and is very close to that of an emission band (at about 3.424 eV) associated with the presence of oxygen impurities reported previously by Chung *et al.*<sup>19</sup> There, the intensity of this emission band was found to be strongly dependent on the oxygen implantation dosage. It has been pointed out that oxygen impurities may also act as substitutional donors.<sup>19,27</sup> In the case presented here, the 3.42 eV transition could be associated with the presence of other substitutional donors as well, which would show up at about the same energy position. We have assigned the emission band near 3.42 eV to the recombination between electrons bound to substitutional donor impurities and free holes, the band to impurity, or the  $(D^0, h^+)$  transition as proposed by Chung *et al.*<sup>19</sup> Other transition mechanisms, including donor–acceptor-pair (DAP) recombination and the recombination between the free electrons and neutral acceptors, are unlikely as discussed previously.<sup>24</sup> For the  $(D^0, h^+)$  transition, the emitted energy is  $h\nu = E_g - E_D$  at low excitation intensities at 0 K. From the energy position of the emission line (3.420 eV) and the energy gap  $E_g$  of GaN at low temperatures of about 3.503 eV,<sup>20,28</sup> we obtain a binding energy of  $E_D = 83 \text{ meV}$  for the substitutional donors in GaN. Our results obtained for the two samples investigated here indicate that the presence of substitutional donor impurities has very little correlation with the high room temperature free carrier concentration observed in GaN, given the fact that the donor impurity related emission near 3.420 eV is very weak in sample A, although the room temperature free carrier concentration in sample A is higher than that in sample B (see Table I). This interpretation is also consistent with the fact that the binding energy

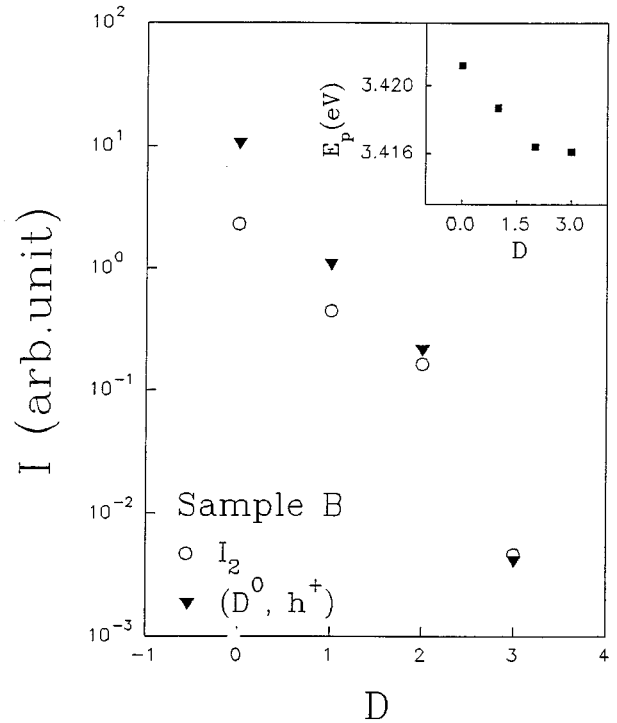


FIG. 4. Semilogarithmic plot of integrated photoluminescence intensities of the  $I_2$  and the  $(D^0, h^+)$  emission lines observed in sample B as functions of the excitation intensity attenuated parameter  $D$ . The inset shows the spectral peak position  $E_p$  of the  $(D^0, h^+)$  emission line as a function of  $D$ .

of the substitutional donor impurities observed here is much larger than a value of about 30 meV (Ref. 28) for the  $N$  vacancies which are responsible for the high native donor defect concentration in GaN.

Several features can be observed from Fig. 3. For the  $I_2$  transition, both the peak position and FWHM are independent of excitation intensity. The sharpest feature in Fig. 3 is the relative intensity ratio of the  $I_2$  to the  $(D^0, h^+)$  emission line. The  $I_2$  transition is the dominant emission line at low excitation intensities. As excitation intensity increases ( $D$  decreases), the relative emission intensity of the  $(D^0, h^+)$  transition increases. At  $D=0$ , the emission intensity of the  $(D^0, h^+)$  transition is almost an order of magnitude higher than that of the  $I_2$  transition. We want to indicate that the absolute emission intensities for both of these emission lines increase with an increase of excitation intensity. This is illustrated in Fig. 4, which shows a semilogarithmic plot of the integrated photoluminescence intensities of the  $I_2$  and the  $(D^0, h^+)$  emission lines observed in sample B as functions of the excitation intensity attenuated parameter  $D$ . We see that the luminescence intensities of both emission lines increase approximately linearly with excitation intensity. However, the intensity increase rate for the  $(D^0, h^+)$  transition is larger than that for the  $I_2$  transition. The inset shows the spectral peak positions of the  $(D^0, h^+)$  emission line,  $E_p$ , as a function of  $D$ , which indicates that  $E_p$  increases with excitation intensity. A total shift of about 5 meV is observed when the excitation intensity is changed by 3 orders of magnitude. This is expected for the band-to-impurity transition, which involves the participation of free holes. As the excita-

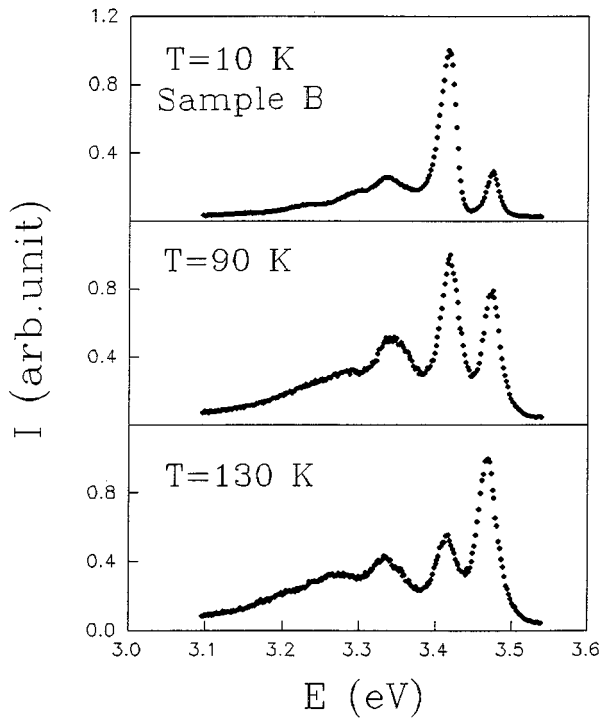


FIG. 5. cw photoluminescence spectra of sample B measured at three representative temperatures at an excitation intensity  $D=0$ . Each spectrum has been normalized to its maximum emission intensity.

tion intensity increases, the free hole concentration and hence the quasi-Fermi level of the free holes also increase, which will result in a spectral peak position shift to higher energies.<sup>29–31</sup> On the other hand, the peak position is also expected to shift toward lower energies as the delay time increases due to the decrease of the free hole concentration or the quasi-Fermi level, which will be discussed later.

Figure 5 shows the luminescence emission spectra of sample B obtained at three representative temperatures. The absolute emission intensities for all emission lines shown in Fig. 5 decrease with increasing temperature. However, the relative intensity ratio of the  $I_2$  to the  $(D^0, h^+)$  emission line increases with an increase of temperature. At temperatures above 100 K, the integrated intensity of the  $I_2$  line actually decreases more rapidly with temperature than the  $(D^0, h^+)$  line. In Fig. 6, we have plotted in a semilogarithmic scale the integrated intensity of (a) the  $I_2$  and (b) the  $(D^0, h^+)$  emission lines versus the reciprocal of temperature (Arrhenius plot), which shows a steeper slope for the  $I_2$  transition at above 100 K. At the high temperature region, both the  $I_2$  and  $(D^0, h^+)$  emission intensities show an activated behavior.

The spectral peak positions of the three observed emission lines shown in Fig. 5 all shift toward lower energies as temperature increases. For a clear presentation, we have plotted in Fig. 7 the temperature dependencies of the spectral peak positions for these three emission lines. The emission line at about 3.34 eV (when  $T=10$  K) disappears at temperatures above 150 K. The temperature dependence of the  $I_2$  emission line is identical to that observed in sample A and can be described by the energy gap variation with tempera-

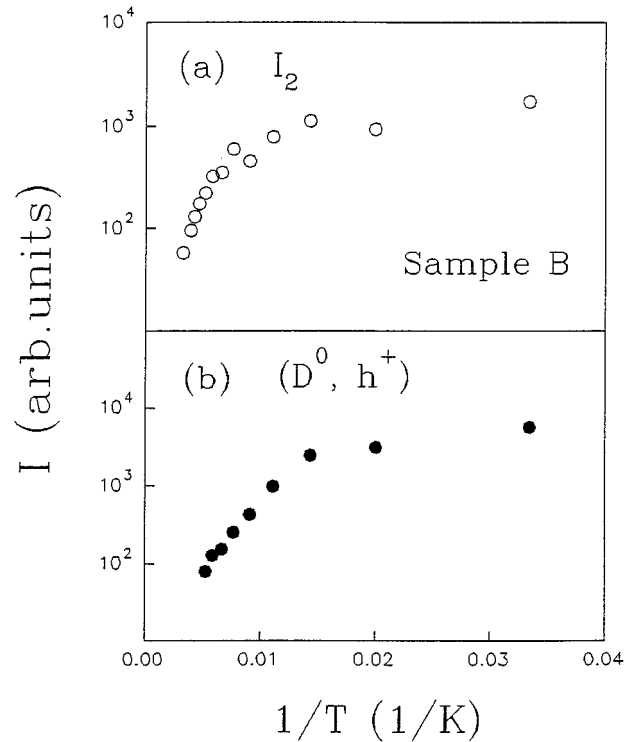


FIG. 6. Arrhenius plots of the integrated luminescence intensities of (a) the  $I_2$  and (b)  $(D^0, h^+)$  emission lines in sample B.

ture. In sharp contrast, the  $(D^0, h^+)$  and the third emission lines at around 3.34 eV do not follow the variation of the band gap with temperature. As a result, the spectral peak separation between the  $I_2$  and the  $(D^0, h^+)$  emission lines,  $\Delta E$ , decreases monotonically with temperature, as Fig. 8 illustrates. The inset of Fig. 8 shows the spectral peak separation between the  $(D^0, h^+)$  and the third emission lines,  $\delta E$ , which is a constant throughout the investigated temperature range, which seems to suggest that the  $(D^0, h^+)$  and the third emission lines are of the same physical origin, i.e., the 3.338 eV line is either a phonon replica of the  $(D^0, h^+)$  emission line or another  $(D^0, h^+)$  transition. However,  $\delta E$  is about 75 meV, which is different from the currently accepted values of the LO phonon energy of 92 meV and the TO phonon energy of 70 meV. This seems to suggest that the 3.338 eV line is due to another  $(D^0, h^+)$  transition. Time-resolved measurements seem to indicate that the 3.338 eV emission line may have a longer recombination lifetime. However, due to the presence of the broadbands resulting from the DAP recombination at the low energy side, we are unable to comment on whether the two emission lines at 3.420 and 3.338 eV have the same or different dynamical behaviors from time-resolved measurements. Further investigation is needed to identify the origin of the 3.338 eV emission line.

The properties of the band-to-impurity transitions,  $(D^0, h^+)$  and  $(A^0, e^-)$ , in CdS have been studied previously by Colbow.<sup>29</sup> The temperature dependence of the spectral peak position of the  $(D^0, h^+)$  transition can be written as

$$E(D^0, h^+) = E_G - E_D + kT, \quad (4)$$

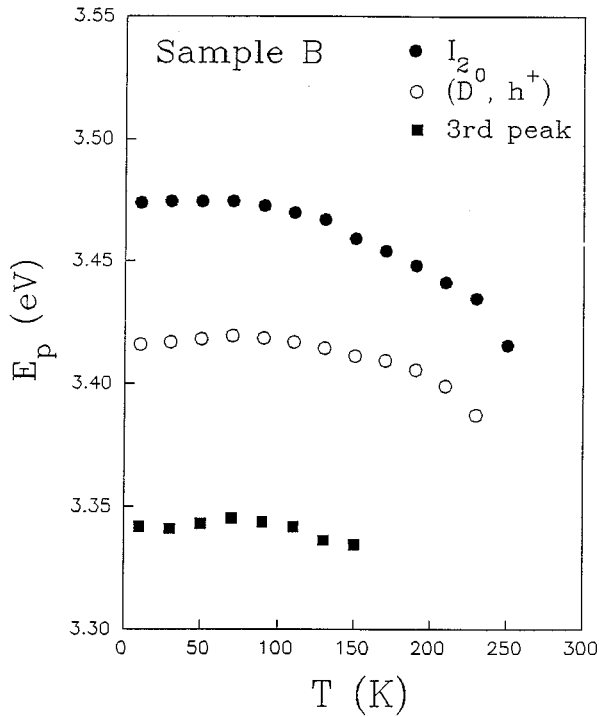


FIG. 7. The temperature dependencies of the three dominant luminescence spectra peak positions of sample B.

where  $E_G$  and  $E_D$  are energy gap and donor binding energy, respectively. The third term,  $kT$ , in Eq. (4) is due to the kinetic energy and the energy dependence of the transition probability of free holes in bulk materials. The peak energy position of the  $I_2$  transition is

$$E(I_2) = E_G - E_x - E_{bx}, \quad (5)$$

where  $E_x$  and  $E_{bx}$  are the binding energies of free exciton and donor-bound exciton, respectively. Thus from Eqs. (4) and (5), the temperature dependence of the spectral peak separation between the  $I_2$  and the  $(D^0, h^+)$  transition lines,  $\Delta E$ , can be written as

$$\Delta E = E(I_2) - E(D^0, h^+) = E_D - E_x - E_{bx} - kT, \quad (6)$$

which shows that  $\Delta E$  decreases linearly with temperature with the slope being the Boltzmann constant  $k$  since  $E_D$ ,  $E_{bx}$ , and  $E_x$  are independent of temperature.

Equation (6) also indicates that  $\Delta E = E_D - E_x - E_{bx}$  at  $T=0$  K. By extrapolating the data points in Fig. 8 to 0 K, we obtain a value for  $\Delta E$  of 58.7 meV at  $T=0$  K. On the other hand, by taking the binding energy of  $D^0$  to be 83 meV as obtained from Fig. 3 and the binding energies of free exciton ( $E_x$ ) and donor-bound exciton ( $E_{bx}$ ), respectively, to be 19 and 7 meV as obtained for other superior quality GaN layers deposited by the most recent MBE and MOCVD techniques,<sup>21,22</sup> we obtain a value of  $\Delta E$  of 57 meV at 0 K. The consistency in  $\Delta E$  obtained by the two different measurements provides additional solid evidence for the assignment of the 3.420 eV emission line as a band-to-impurity transition. Since the  $(A^0, e^-)$  transition can be excluded by

considering the energy position of the emission line, the emission line near 3.42 eV can be conclusively assigned to the  $(D^0, h^+)$  transition.

However, the slope of the spectral peak separation ( $\Delta E$ ) versus temperature plot shown in Fig. 8 is not  $k$ , instead it is close to  $0.5k$ . One of the possible causes is the two-dimensional (2D) motion of free holes in the epitaxial layer instead of uniform three-dimensional (3D) motion in bulk materials. We have repeated Colbow's calculation for the  $(D^0, h^+)$  transition by considering both 2D and 3D motions and we obtain an expression for its peak position as

$$E(D^0, h^+) = E_G - E_D + \alpha kT, \quad (7)$$

where  $\alpha=0.5$  and 1 for the 2D layer and 3D bulk materials, respectively. From this, we thus have,

$$\Delta E = E_D - E_x - E_{bx} - \alpha kT. \quad (8)$$

The slope obtained from the least-squares fit between data points in Fig. 8 and Eq. (8) is  $0.58k$ , which indicates that the  $(D^0, h^+)$  transition observed in the epitaxial layer is different from that in the bulk. Our results show that the motion of free holes is mainly constrained in the plane of the epitaxial layer at temperatures below 140 K. However, the free hole motion along the  $z$  axis (growth direction) is not completely precluded, which shows up as  $\alpha$  being slightly larger than 0.5.

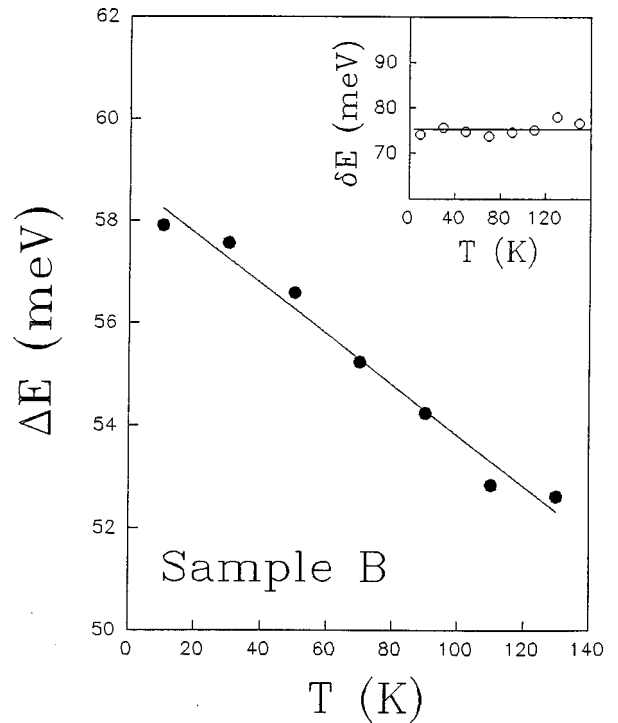


FIG. 8. The temperature dependence of the energy separation between the  $I_2$  and the  $(D^0, h^+)$  emission peaks,  $\Delta E$ , in sample B. The solid line is the least-squares fit of data with Eq. (8). The inset shows the temperature dependence of the energy separation between the  $(D^0, h^+)$  and the third emission peak (near 3.338 eV),  $\delta E$ , in which the solid line is a guide to the eyes indicating that  $\delta E$  is a constant value of about 75 meV.

## B. Time-resolved photoluminescence spectra and recombination dynamics

### 1. Time-resolved emission spectra

Time-resolved emission spectroscopy has been employed to study the dynamics of the  $I_2$  and the band-to-impurity transitions. We find that the recombination lifetime of the  $I_2$  transition is about 0.1 ns in the samples investigated here. Due to high impurity concentrations, its systematic dependence on temperature and excitation intensity cannot be obtained in these samples. We concentrate our time-resolved luminescence study on the  $(D^0, h^+)$  transition in sample B. Figure 9 shows a semilogarithmic plot of the temporal response of the  $(D^0, h^+)$  transition measured near its peak position at  $T=10$  K. The system response to the laser pulses (7 ps) has been indicated as “system,” which was used for the deconvolution of raw data. The wiggling line is the experimental data, while the solid line is the least-squares fit of single exponential decay with the deconvolution of system response. The residual of the least-squares fit is also included in the bottom of Fig. 9. As we can see, the decay of the  $(D^0, h^+)$  transition in GaN is a single exponential,  $I(t) = I_0 e^{-t/\tau}$ , with  $\tau$  being the recombination lifetime. We have measured the luminescence temporal responses such as that shown in Fig. 9 at different emission energies covering the entire emission band (see Fig. 11) as well as at different temperatures from 10 to 150 K (see Fig. 12). In all cases, the decay of the luminescence is single exponential.

Figure 10 shows the time-resolved emission spectra of the  $(D^0, h^+)$  transition measured at  $T=10$  K for several representative delay times. Here, the delay time  $t=0$  has been chosen at the positions of maximum intensity in the luminescence temporal responses such as that shown in Fig. 9. The arrows in Fig. 10 indicate the spectral peak positions at different delay times. Several features can be observed from Fig. 10. First, the peak positions of the emission line shift toward lower energies with an increase of delay time. Second, the linewidth of the emission band also increases with delay time. Third, the luminescence decays faster at higher emission energies than at lower emission energies, which is due to the nature of this transition line as discussed previously.<sup>24</sup>

### 2. Recombination lifetimes

The emission energy dependence of the recombination lifetime for the  $(D^0, h^+)$  emission line is depicted in Fig. 11 which shows that the lifetime ( $\tau$ ) is of the order of subnanoseconds and decreases with an increase of emission energy. From Fig. 11, the upper limit value of the radiative recombination lifetime of the  $(D^0, h^+)$  transition associated with substitutional donor impurities is about 1 ns at 10 K in GaN, which is shorter than the typical lifetime of the order of several nanoseconds for this type of transition in better studied materials such as doped GaAs.<sup>31</sup> If the  $(D^0, h^+)$  emission line involves only a single impurity energy level, the dependence of the recombination lifetime on emission energy is not expected. The results obtained here clearly indicate that the binding energy  $E_D$  of the donor involved for the  $(D^0, h^+)$  transition has a distribution. The behavior ob-

served here is most likely due to the binding energy dependence of the radiative recombination rate, i.e., the behavior of  $\tau(E)$  is associated with the distribution of the donor binding energy,  $E_D$ .

By assuming shallow, discrete, and nonoverlapping impurities, the maximum transition probabilities for the  $(D^0, h^+)$  transitions at 0 K have been calculated previously,<sup>30,31</sup> which showed that the radiative recombination lifetime of a band-to-impurity transition depends on  $E_D$  and can be described by,  $\tau \propto E_D^{3/2} \propto (E_g - h\nu)^{3/2}$ , with  $h\nu$  being the emission energy  $E$ . Experimentally observed emission energy dependence of the recombination lifetime of the  $(D^0, h^+)$  transition measured in the entire emission band can be described well by

$$\tau = A(E_0 - E)^{3/2}, \quad (E \leq E_0) \quad (9)$$

as shown by the solid curve in Fig. 11, where the fitted values for  $E_0$  and  $A$  are 3.454 eV and 68.9 ns/eV<sup>1.5</sup>, respectively. The reason for the difference between the fitted value of  $E_0$  and  $E_g$  is not clear at this stage.

The temperature dependence of the recombination lifetime of the  $(D^0, h^+)$  transition has also been measured in the temperature range between 10 and 150 K at their corresponding emission peak positions and Fig. 12 shows the result. At temperatures below 50 or above 120 K, the lifetime is independent of temperature, suggesting very efficient radiative recombination at low temperatures, in agreement with the results of Fig. 4. However, a strong temperature dependent lifetime is observed in the temperature range between 50 and 100 K.  $\tau$  changed rapidly in this temperature region and varied from 0.63 to about 0.3 ns.

This behavior can be accounted for by an increased nonradiative recombination rate at a higher temperature. The temperature dependence of the nonradiative decay rate can be described by  $\gamma_{\text{non}} = \gamma_0 \exp(-E_0/kT)$ , where  $\gamma_0$  and  $E_0$  are the nonradiative decay rate at the limit of  $T \rightarrow \infty$  and the activation energy of the nonradiative process of the  $(D^0, h^+)$  transition. If we further assume that the radiative recombination rate,  $\gamma_r$ , of the  $(D^0, h^+)$  transition is independently of or weakly dependent on temperature, then the measured recombination lifetime of the  $(D^0, h^+)$  transition is described by

$$\tau = [\gamma_r + \gamma_0 \exp(-E_0/kT)]^{-1}. \quad (10)$$

Equation (10) has been used to fit experimentally measured  $\tau$  as shown in Fig. 12 and cannot fit the data. Instead, in the entire temperature range investigated here, the measured recombination lifetime  $\tau$  can be fitted very well by the form

$$\tau = [\gamma_r + \gamma_0 \exp(-E_0/kT)]^{-1} + C, \quad (11)$$

as shown as the solid curve in Fig. 12. The fitted values are  $\gamma_r = 2.9 \text{ ns}^{-1}$ ,  $\gamma_0 = 2.9 \times 10^5 \text{ ns}^{-1}$ , and  $E_0 = 78.5 \text{ meV}$ . This behavior seems to suggest that at temperatures above 50 K, the total lifetime is determined by both radiative and nonradiative recombination. The activation energy  $E_0$  obtained here is very close to the binding energy of the donor,  $E_D = 83 \text{ meV}$ , which implies that the nonradiative process of the  $(D^0, h^+)$  transition is caused by thermal dissociation of

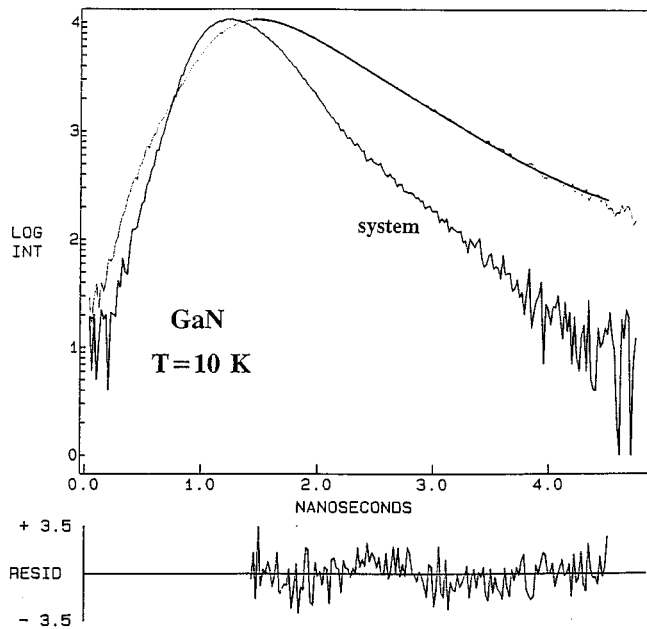


FIG. 9. The semilogarithmic plot of the temporal response of the band-to-impurity emission line in sample B measured near its peak position at  $T=10$  K. The instrument response to laser pulses (7 ps width) is indicated as “system” and the wiggling line is the experimental data. The solid line is the least-squares fit using a single exponential decay with the deconvolution of the instrumental response. The residues of the least-squares fit are also included in the bottom. The excitation photon energy was 4.260 eV.

$D^0$ . This is also consistent with the result of thermal quenching of the  $(D^0, h^+)$  emission intensity shown in Fig. 6.

The fitted value of  $C$  is 0.3 ns. This constant term of 0.3 ns in Eq. (11) is a little difficult to justify. The best explanation we have in this stage is that it may be related to carrier transformation from other recombination channels, by such processes as the decay of the bound-exciton ( $I_2$ ) into the  $(D^0, h^+)$  recombination channel. If this is the case, the decay of the  $(D^0, h^+)$  transition will be determined by this transfer time at high temperatures if this time is the longest among the radiative and nonradiative recombination lifetimes and the transfer time. A value of 0.3 ns is reasonable for this transfer process.

#### IV. CONCLUSIONS

In conclusion, we have studied photoluminescence properties near the band-edge under different conditions for  $n$ -type GaN epitaxial layers grown by plasma assisted MBE. For the sample grown at a lower growth rate, an emission line of about 83 meV below the band gap has been observed in addition to the well-known neutral-donor-bound exciton ( $I_2$ ) transition. This emission line has been assigned to the  $(D^0, h^+)$  transition associated with the presence of substitutional donor impurities. The temperature dependence of the peak position has confirmed such an assignment. Time-resolved emission spectroscopy has also been employed to study the carrier dynamics of this transition. The decay of this emission line is found to be exponential with lifetimes on the subnanosecond scale. The emission energy and tem-

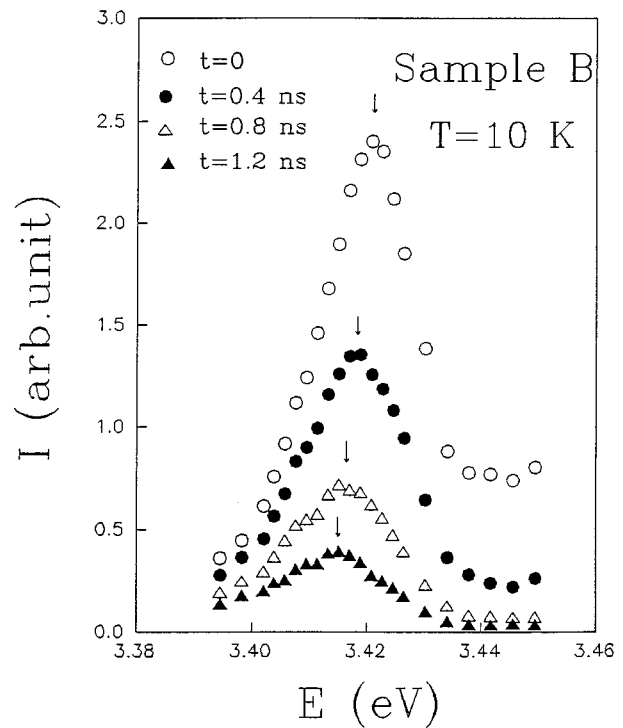


FIG. 10. Time-resolved photoluminescence spectra of the  $(D^0, h^+)$  emission line in sample B measured at  $T=10$  K. The arrows indicate the spectral peak positions at different delay times. Delay time  $t=0$  has been chosen at the positions of the maximum intensity in the luminescence temporal responses such as that shown in Fig. 9.

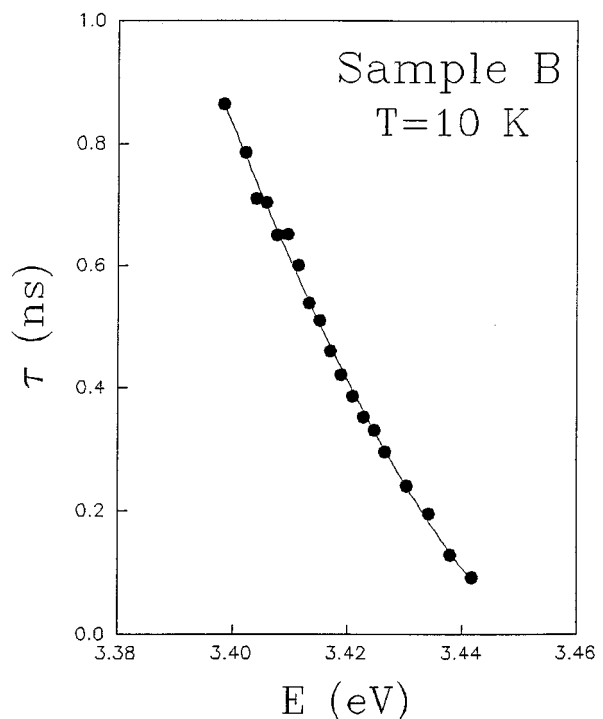


FIG. 11. The emission energy dependence of the recombination lifetime of the  $(D^0, h^+)$  emission line in sample B measured at  $T=10$  K. The solid line is the least-squares fit of experimental data by using Eq. (9).

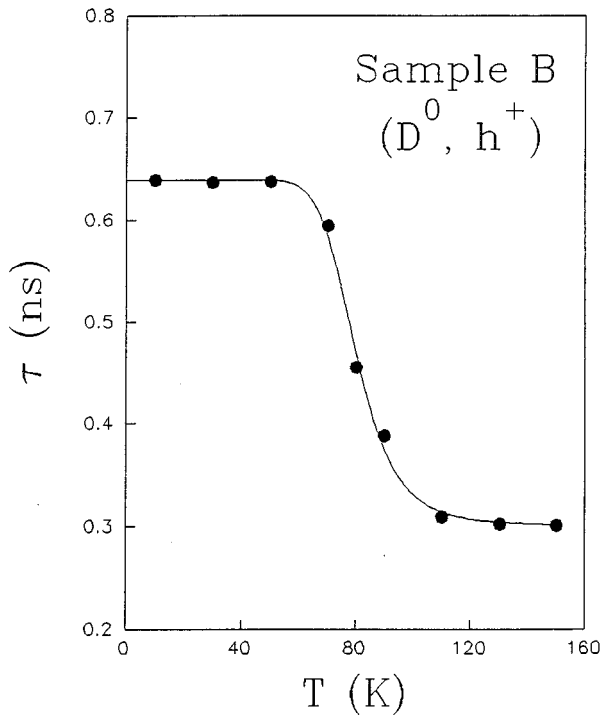


FIG. 12. The temperature dependence of the recombination lifetime  $\tau$  of the  $(D^0, h^+)$  emission line in sample B measured at spectral peak positions. The solid line is the least-squares fit of experimental data by using Eq. (11).

perature dependencies of the recombination lifetime have been measured. Our results indicate that the binding energy of the donor impurities has a distribution. Additionally, the absence of the  $(D^0, h^+)$  emission line in the sample with a higher room temperature free carrier concentration indicates that the possibility of substitutional donor impurities being responsible for high free carrier concentrations in GaN can be precluded. Our results also show that the motion of free holes in epitaxial layers is restricted mostly in the growth plane at temperatures below 140 K, which would modify an existing theory for the band-to-impurity transitions in bulk materials.

#### ACKNOWLEDGMENTS

J.Y.L. and H.X.J. are thankful for insightful discussions and the encouragement of Dr. John Zavada. A.S., B.N.S.,

A.B., and H.M. would like to acknowledge the support of the office of Naval Research under Grant No. N00014-89-J-1780 and thank Max Yoder for support.

- <sup>1</sup> *Wide Bandgap Semiconductors*, edited by T. D. Moustakas, J. I. Pankove, and Y. Hamakawa (Materials Research Society, Pittsburgh, PA, 1992), Vol. 242.
- <sup>2</sup> S. Strite, M. E. Lin, and H. Morkoç, *Thin Solid Films* **231**, 197 (1993).
- <sup>3</sup> J. I. Pankove, *Mater. Res. Soc. Symp. Proc.* **97**, 409 (1987).
- <sup>4</sup> S. Nakamura, M. Senoh, and T. Mukai, *Jpn. J. Appl. Phys.* **32** L8 (1993).
- <sup>5</sup> M. A. Khan, A. Bhattarai, J. N. Kuznia, and D. T. Olson, *Appl. Phys. Lett.* **63**, 1214 (1993).
- <sup>6</sup> S. Strite and H. Morkoç, *J. Vac. Sci. Technol. B* **10**, 1237 (1992).
- <sup>7</sup> S. Nakamura, T. Mukai, and M. Senoh, *Appl. Phys. Lett.* **74**, 1687 (1994).
- <sup>8</sup> M. Asif Khan, J. N. Kuznia, D. T. Olson, W. J. Schaff, J. W. Burm, and M. S. Shur, *Appl. Phys. Lett.* **65**, 1121 (1994).
- <sup>9</sup> C. Binari, L. B. Rowland, W. Kruppa, G. Kelner, K. Doverspike, and D. K. Gaskill, *Electron. Lett.* **30**, 1248 (1994).
- <sup>10</sup> J. I. Pankove, J. E. Berkeyheiser, H. P. Maruska, and J. Wittke, *Solid State Commun.* **8**, 1051 (1970).
- <sup>11</sup> R. Dingle and M. Illegems, *Solid State Commun.* **9**, 175 (1971).
- <sup>12</sup> R. Dingle, D. D. Sell, S. E. Stokowski, and M. Illegems, *Phys. Rev. B* **4**, 1211 (1971).
- <sup>13</sup> R. Dingle, D. D. Sell, S. E. Stokowski, P. J. Dean, and M. Illegems, *Phys. Rev. B* **3**, 497 (1971).
- <sup>14</sup> B. Monemar, *Phys. Rev. B* **10**, 676 (1974).
- <sup>15</sup> J. M. Hvam and E. Ejder, *J. Lumin.* **12/13**, 611 (1976).
- <sup>16</sup> R. Dai, S. Fu, J. Xie, G. Fan, G. Hu, H. Schrey, and C. Klingshirn, *J. Phys. C* **15**, 393 (1982).
- <sup>17</sup> H. G. Grimmeiss and B. Monemar, *J. Appl. Phys.* **41**, 4054 (1970).
- <sup>18</sup> K. Naniwae, S. Itoh, H. Amano, K. Itoh, K. Hirematsu, and I. Akasaki, *J. Cryst. Growth* **99**, 381 (1990).
- <sup>19</sup> B. C. Chung and M. Gershenson, *J. Appl. Phys.* **72**, 651 (1992).
- <sup>20</sup> W. Shan, T. J. Schmidt, X. H. Yang, J. J. Song, and B. Goldenberg, *Appl. Phys. Lett.* **66**, 985 (1995).
- <sup>21</sup> M. Smith, G. D. Chen, J. Z. Li, J. Y. Lin, H. X. Jiang, A. Salvador, W. Kim, O. Aktas, A. Botchkarov, and H. Morkoç, *Appl. Phys. Lett.* **67**, 3387 (1995).
- <sup>22</sup> M. Smith, G. D. Chen, J. Y. Lin, H. X. Jiang, M. A. Khan, and J. Sun (to be published).
- <sup>23</sup> G. D. Chen, M. Smith, J. Y. Lin, H. X. Jiang, M. A. Khan, and J. Sun, *Appl. Phys. Lett.* **67**, 1653; **67**, 3295 (1995).
- <sup>24</sup> M. Smith, G. D. Chen, J. Y. Lin, H. X. Jiang, A. Salvador, B. N. Sverdlov, A. Botchkarov, and H. Morkoç, *Appl. Phys. Lett.* **66**, 3474 (1995).
- <sup>25</sup> S. Rudin, T. L. Reinecke, and B. Segall, *Phys. Rev. B* **42**, 11218 (1990).
- <sup>26</sup> V. Srinivas, Y. J. Chen, and C. E. C. Wood, *Solid State Commun.* **89**, 611 (1994).
- <sup>27</sup> W. Wiefert, R. Fanzhelal, E. Butter, H. Sobotta, and V. Riede, *Cryst. Res. Technol.* **18**, 383 (1993).
- <sup>28</sup> Landolt-Börnstein, *Numerical Data and Functional Relationships in Science and Technology*, edited by P. Eckerlin and H. Kandler (Springer, Berlin, 1971), Vol. III.
- <sup>29</sup> K. Colbow, *Phys. Rev.* **141**, 742 (1966).
- <sup>30</sup> W. P. Dumke, *Phys. Rev.* **132**, 1998 (1963).
- <sup>31</sup> J. I. Pankove, *Optical Processes in Semiconductors* (Dover, New York, 1971), Chap. 6.